PERGAMON

International Journal of Heat and Mass Transfer 44 (2001) 3431–3442

International Journal of HEAT and MASS TRANSFER

www.elsevier.com/locate/ijhmt

Liquid steel flow, heat transfer and solidification in mold of continuous casters during grade transition

X.K. Lan [1], J.M. Khodadadi *

Mechanical Engineering Department, Auburn University, 201 Ross Hall, Auburn, AL 36849-5341, USA

Received 1 June 2000; received in revised form 27 November 2000

Abstract

A computational study of the unsteady axisymmetric turbulent liquid steel flow, heat transfer and solidification in continuous casting molds during the grade transition operation is presented. The computations are based on an iterative, finite-volume numerical procedure using primitive dependent variables, whereby the governing time-dependent continuity, momentum and energy equations in combination with a low-Reynolds number turbulence model are solved. A single-domain enthalpy formulation is used for simulation of the phase change phenomenon. Darcy's Law-type porous media treatment is used to account for the effect of phase change on convection. In spite of the transient nature of the incoming liquid steel velocity, increase in size of the liquid pool is not significant, whereas the increase of the volume of the mushy zone is marked and is as much as 48% relative to its initial size. Distinct temperature rise signatures on the surface of the casting were detected. The heat removal rate from the mold increases almost linearly similar to the ramping of the casting speed. Thinning of the solidified shell during tundish change is significant and must be taken into account in practice to prevent breakout.

1. Introduction

In recent years, the continuous casting process in which molten metal is constantly cast into semi-finished shapes has been widely adopted in the steel and non-ferrous metal producing industry. The mold is one of the most important components of a continuous caster (Fig. 1). The liquid metal which flows through the nozzle originates from an intermediate holding chamber called a tundish, which itself is supplied by a much bigger container known as a ladle. Fluid flow and thermal modeling studies of molten flow in ladles and tundishes which do not involve phase change have been reported. An understanding of transport processes in the liquid metal pool within the mold is of particular importance because it can be used in controlling the growth rate of the solidifying shell, thus affecting the microstructure of the final casting. The transport processes also control the formation of various defects which can hamper subsequent processing. Examples of defects formed in this region are macrosegregation, surface irregularities, such as cold folding and oscillation marks, and more serious defects such as longitudinal or transverse cracks. A more catastrophic problem which may occur is "breakout", where the shell ruptures and molten metal is discharged in an uncontrolled manner.

2. Review of literature

Szekely and Yadoya [1] investigated the flow field in the mold region of continuous casters by performing flow visualization and velocity measurements in a water model. The existence of a turbulent recirculatory motion in the upper part was verified. The penetration length of the separated zone in the system approached 4–6 mold diameters. Szekely and Yadoya [2] gave the theoretical description of the velocity and temperature fields in the

* Corresponding author. Tel.: +1-334-844-3333; fax: +1-334-844-3307.

E-mail address: jkhodada@eng.auburn.edu (J.M. Khodadadi).

[1] Present address: Beloit Corporation, 1165 Prairie Hill Road, Rockton, IL 61072-1595, USA.

0017-9310/01/$ - see front matter
PII: S0017-9310(01)00005-9

Nomenclature

c_p	specific heat (J/kg K)
C_0	Darcy coefficient (kg/s m^3)
d_j	jet diameter (m)
g	gravitational acceleration (m/s^2)
Gr	Grashof number, defined as $g\beta(2R)^3(T_{ref} - T_s)/v^2$
P	pressure (Pa)
Pr	Prandtl number, defined as $\mu c_p/k$
r_j	radius of the jet (m)
R	radius of the mold (m)
t	time (s)
T	temperature (K)
T_a	ambient temperature (K)
T_j	jet's exit temperature (K)
T_{ref}	reference temperature, defined as jet's exit temperature (K)
T_w	temperature of the surface of casting (K)
U_c	casting speed (m/s)
U_j	jet's uniform exit velocity (m/s)

Greek symbols

β	thermal expansion coefficient (K^{-1})
κ	thermal conductivity (W/m K)
μ	dynamic viscosity of the fluid (N s/m^2)
v	kinematic viscosity of the fluid (m^2/s)
ρ	density of the fluid (kg/m^3)

Subscripts

j	related to the jet
t	turbulent

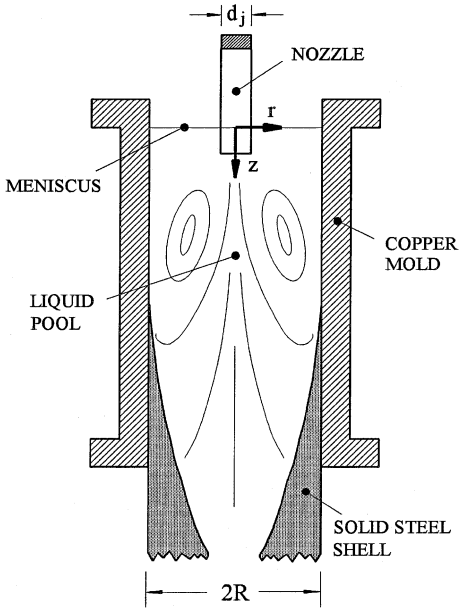

Fig. 1. Molten metal flow inside the mold.

mold region, by solving vorticity-stream function-based equations combined with a one-equation turbulence model. Khodadadi et al. [3] have reported results of flow visualization studies (tuft grid, dye tracer and hydrogen bubble techniques) in an aqueous system using both straight-through and radial-entry nozzles. The coupled turbulent flow and heat transfer equations accounting for buoyancy, surface tension and phase change were solved by Shyy et al. [4] in order to simulate the titanium alloy continuous ingot casting in an electron beam melting process. A Darcy's Law-type of porous media treatment was utilized to account for the effect of phase change on convection. Shyy et al. [5] extended their previous work [4] to study the effect of correlation fluctuations between velocity and temperature, in addition to correlated fluctuations between velocity and release of latent heat on temperature contours and phase change. Coupled turbulent flow, heat and solute transport in the mold of a continuous billet caster was studied numerically for steady-state operating conditions by Reza Aboutalebi et al. [6]. Using a low-Reynolds number turbulence model and a continuum model for treatment of various phases, they studied the effects of the casting speed, steel grade, nozzle configuration on the flow field, solidification pattern and carbon segregation for a binary Fe–C alloy system. The trajectory of inclusions and their density distributions were calculated and reasonable agreements with measurements were reported. A computational study of the transient axisymmetric turbulent fluid flow, heat transfer and solidification in the mold of a round steel bloom caster during the ladle change practice was recently reported by Lan and Khodadadi [7]. The study was motivated by the greater industrial attention to quality improvement associated with unsteady-state slab portions which mainly correspond to ladle change. It was shown that due to the time-dependence of the jet temperature during the ladle change, the volume occupied by the liquid phase generally expanded in the radial direction during each cycle, whereas the axial extent of the liquid pool shrank due to the greater influence of the buoyancy force. The increase in size for the liquid pool depended on the casting speed and was as much as 25% when compared to the steady-state value, however the size of the mushy zone did not vary greatly over the period of ladle change and the thickness of the solidified shell shrank to some extent during the cycle.

It has become a common practice to continuously cast different grades of steel as successive heats in a single casting sequence. One of the commonly used methods to change the steel grade is the "flying tundish change" practice. In this method, the tundish is changed simultaneously when the ladle is changed to a new grade of steel. As a result, mixing of the two grades in the tundish is eliminated, and the amount of intermixed steel reduced. To accomplish the tundish change, the casting speed must always be slowed down considerably. It is then increased gradually or "ramped" back to its normal setting over several minutes. Huang and Thomas [8] investigated the steel grade transition in a slab caster associated with the flying tundish change process by first solving a steady-state 3-D turbulent flow, then obtaining the velocity field at each time step by uniformly scaling the steady-state velocity solution with the ratio of the current jet velocity to the steady-state value. The velocity field was used for the solution of a 3-D transient species diffusion equation to predict the composition distribution. More recently, Thomas [9] developed a 1-D, transient mathematical model to simulate the final composition distributions produced within continuous-cast slabs and blooms during any arbitrary grade transition. The model was calibrated, and verified with composition measurements on tundish outflow and at the surface and centerlines of slabs and blooms cast during grade transitions. Results show that the amount of intermixed steel generally decreases with lower tundish weight at ladle open, increased holding time before refilling, increased plug flow through the tundish, decreased mold thickness, decreased mold width, casting the most stringent grade first, and using lower average casting speed during the grade change. Ho and Hwang [10] developed a mathematical model to simulate the flow behavior of molten steel in billet continuous casting mold under 3-D turbulent steady flow conditions. The efficiency rate of non-metallic inclusion removal was also estimated. Huang and Thomas [11] recently described initial efforts to develop and apply 3-D finite-difference models to simulate transient flow in the mold without phase change. Predictions of the oscillatory evolution of the flow pattern from biased steady flow to symmetrical steady flow after a sudden change in inlet conditions were given. In addition, the predicted turbulent kinetic energy levels at steady state were shown to correlate with measured surface level fluctuations. These transient phenomena are important because they may lead to defects in the final steel product from entrainment of slag, disruption of solidification at the meniscus and non-uniform heat transfer. In light of the fact that heat transfer and phase change during the grade transition process were not addressed [8,9], the present work was undertaken to study the transient fluid flow of liquid steel, heat transfer and solidification during the flying tundish change process.

3. Computational technique

The computational results presented in this paper were obtained by utilizing the SIMPLE procedure of Patankar [12]. The elliptic time-averaged transport equations governing this time-dependent axisymmetric problem of the flow of an incompressible Newtonian fluid are of the general form

$$\frac{\partial(\rho\phi)}{\partial t} + \nabla\cdot(\rho\mathbf{V}\phi) = \nabla\cdot(\Gamma_\phi\nabla\phi) + S^\phi, \tag{1}$$

where $\mathbf{V}$ is the velocity vector with its two components U and V representing the time-averaged velocities in the axial (z) and radial (r) directions, respectively. Due to the axisymmetric nature of the problem, tangential gradients vanish. The variable ϕ represents various time-averaged quantities, i.e., mean velocities, enthalpy, turbulence kinetic energy (k) and turbulence energy dissipation rate (ε). The quantities Γ_ϕ and S^ϕ represent the diffusivity of ϕ and the source term for various transport equations, respectively, all of which are summarized in Table 1.

3.1. Turbulence model

The low-Reynolds number k–ε turbulence model of Lam and Bremhorst [13] in combination with the suggested turbulence energy dissipation rate boundary condition of Patel et al. [14] were utilized. The experimental and computational work of Lan et al. [15] showed that among five variations of low-Reynolds number k–ε turbulence models, the Lam and Bremhorst model performs very well in predicting the velocity and turbulence fields in submerged jets which involve complex reverse flow and are directly relevant to the flow in continuous casting molds. Detailed comparison of the computed velocity and turbulence information to the non-invasive laser Doppler velocimeter measurements were provided [15].

3.2. Phase change model

The *enthalpy formulation* which belongs to the single-region (or continuum) class of methods was used. The present form of the source term for the thermal energy equation in Table 1 can be derived by splitting the total enthalpy of the material into the sensible enthalpy ($h = c_\mathrm{p}T$) and the latent heat (H) [16,17]. A linear relationship between the latent heat and temperature is used, i.e.,

$$H = f_\ell H_\mathrm{f}, \tag{2}$$

where H_f is the latent heat of the phase change and the liquid fraction (f_ℓ) is given by

$$f_\ell = \begin{cases} 1 & T > T_\ell, \\ \frac{T-T_\mathrm{s}}{T_\ell-T_\mathrm{s}}, & T_\mathrm{s} \leqslant T \leqslant T_\ell, \\ 0, & T < T_\mathrm{s}, \end{cases} \tag{3}$$

Table 1
Transport equations

Equations	Variables		
	ϕ	Γ_ϕ	S^ϕ
Continuity	1	0	0
Axial momentum	U	μ_{eff}	$\frac{\partial}{\partial z}\left(\mu_{\text{eff}}\frac{\partial U}{\partial z}\right)+\frac{1}{r}\frac{\partial}{\partial r}\left(r\mu_{\text{eff}}\frac{\partial V}{\partial z}\right)-\frac{\partial P}{\partial z}+\rho g\beta(T_{\text{ref}}-T)+A(U-U_{\text{c}})$
Radial momentum	V	μ_{eff}	$\frac{\partial}{\partial z}\left(\mu_{\text{eff}}\frac{\partial U}{\partial r}\right)+\frac{1}{r}\frac{\partial}{\partial r}\left(r\mu_{\text{eff}}\frac{\partial V}{\partial r}\right)-\frac{\partial P}{\partial r}-2\mu_{\text{eff}}\frac{V}{r^2}+AV$
Thermal energy	h	$\mu/Pr+\mu_{\text{t}}/Pr_{\text{t}}$	$G-\frac{\partial(\rho H)}{\partial t}-\nabla\cdot(\rho\mathbf{V}H)-\nabla\cdot(\rho(\mathbf{V}-\mathbf{V}_{\text{c}})(H_{\text{f}}-H))$
Turbulence kinetic energy	k	$\mu+(\mu_{\text{t}}/\sigma_k)$	$G-\rho\varepsilon-\rho D$
Turbulence dissipation rate	ε	$\mu+(\mu_{\text{t}}/\sigma_\varepsilon)$	$\frac{\varepsilon}{k}(C_1 f_1 G-C_2 f_2\rho\varepsilon)+\rho\varepsilon$

$$G=\mu_{\text{t}}\left\{2\left[\left(\frac{\partial U}{\partial z}\right)^2+\left(\frac{\partial V}{\partial r}\right)^2+\left(\frac{V}{r}\right)^2\right]+\left(\frac{\partial U}{\partial r}+\frac{\partial V}{\partial z}\right)^2\right\}=\text{turbulence generation},$$

where $\mathbf{V}_{\text{c}}$ is the casting speed vector, $\mu_{\text{eff}}=\mu+\mu_{\text{t}}$, $\mu=$ dynamic viscosity of the fluid, $\mu_{\text{t}}=\rho C_\mu f_\mu(k^2/\varepsilon)=$ turbulent viscosity, σ_k and σ_ε are effective Prandtl numbers.

$$A=\frac{-C_0(1-f_\ell)^2}{f_\ell^3},\quad Pr_{\text{t}}=1.0.$$

For values of $C_\mu, C_1, C_2, f_1, f_2, f_\mu, \sigma_k, \sigma_\varepsilon, D$ and E, see Table 2.

with T_ℓ and T_{s} being the liquidus and solidus temperatures, respectively. A Darcy's Law-type of porous medium treatment [16] is utilized to account for the effect of phase change on convection. The Darcy terms in the two momentum equations provide extra resistance to flow as the liquid transforms into the solid phase. In order to account for the phase change in the turbulence model, the damping function f_μ in the turbulence model (Table 2) is multiplied by $\sqrt{f_\ell}$ as suggested by Shyy et al. [4].

3.3. Boundary conditions

At the outlet station which was placed 25 mold radii downstream of the inlet plane, the flow was assumed to be fully developed. The radial component of velocity, and the normal gradients of other variables were set to zero at the symmetry axis. Fine grids were placed next to casting surface and with the use of a low-Reynolds number turbulence model, the computations were extended to the surface. On the casting surface next to the

Table 2
Turbulence model constants and terms [13,14]

$C_\mu = 0.09$	$C_1 = 1.44$	$C_2 = 1.92$	
$\sigma_k = 1.0$	$\sigma_\varepsilon = 1.3$	$D=0$	$E=0$

$$f_1=1+\left(\frac{0.05}{f_\mu}\right)^3 \qquad f_2=1-\mathrm{e}^{-(k^2/v\varepsilon)^2}$$

$$f_\mu=\left(1+\frac{20.5}{(k^2/v\varepsilon)}\right)\left[1-\exp(-0.0165(R-r)k^{1/2}/v)\right]^2$$

$$\frac{\partial\varepsilon}{\partial y}=0\quad\text{at the wall } (r=R)$$

mold, the radial velocity component and the turbulence kinetic energy were set to zero. The axial velocity component on the casting surface next to the mold was set according to the following relations:

$$U_{r=R} = 0 \quad \text{for } T_s < T_{r=R}, \tag{4}$$

$$U_{r=R} = U_c \quad \text{for } T_{r=R} \leqslant T_s, \tag{5}$$

with U_c being the casting speed.

The gradient of the turbulence kinetic energy dissipation rate on the casting surface next to the mold was set to zero as suggested by the turbulence model. The boundary conditions used for the energy equation at the casting-mold and casting-spray interfaces were

$$-\kappa \left.\frac{\partial T}{\partial r}\right|_{r=R} = h_1(T_{r=R} - T_a) \quad \text{for } z \leqslant L, \tag{6}$$

$$-\kappa \left.\frac{\partial T}{\partial r}\right|_{r=R} = h_2(T_{r=R} - T_a) \quad \text{for } z > L, \tag{7}$$

where L is the length of the mold. The values of the heat transfer coefficients of the mold and spray (h_1 and h_2) were adopted from Ref. [18]. It is common practice in continuous casting literature to only identify the casting speed (U_c), which refers to the speed of the solidified bloom or slab far downstream. The variation of the jet's exit velocity ($U_j = U_c(R/r_j)^2$) with time during the flying tundish change simulation is shown in Fig. 2. The jet's exit velocity is ramped from 0.64 m/s linearly to 1.28 m/s over a period of 2 min, with the corresponding jet Reynolds numbers, $Re_j = U_j d_j/\nu$ equal to 19,050 and 38,100, respectively. These jet velocity values are equivalent to casting speeds of 1 and 2 cm/s, respectively. The Grashof number was maintained at 6.775×10^9. For the problem at hand which is a *mixed convection* problem, the ratio of $Gr/(Re_j)^2$ determines the importance of buoyancy-driven convection. The values of this ratio were 18.6 and 4.65 at the beginning and conclusion of the ramp period, respectively, which means that buoyancy-driven convection within the mold cannot be ignored. Time zero corresponds to the instant when the new ladle is opened and the new grade of steel starts to flow into the tundish, whereas negative time represents events occurring prior to opening of the new ladle. The simulation was continued for 0.5 min after the casting speed is ramped back to the constant setting of 2 cm/s (jet velocity of 1.28 m/s). Therefore, the total computation time was 2.5 min (150 s). The steady-state solution under the casting speed of 1 cm/s was obtained first and then utilized as the initial conditions for the transient computations. At the inlet plane, the radial component of the jet velocity was set to zero. In the absence of turbulence measurements, uniform values for turbulence kinetic energy and its dissipation rate at the jet exit were assigned according to:

$$k_j = 1.5(0.026U_j)^2, \tag{8}$$

$$\varepsilon_j = C_\mu^{3/4} k_j^{1.5}/(0.09 r_j) \tag{9}$$

which are standard for circular pipe flow situations.

The jet temperature was set to 1530°C (30° of superheat). The geometrical parameters and operating conditions of the caster are summarized in Table 3. Specifically, the value of the Darcy coefficient was adopted in concert with the work of Aboutalebi et al. [6], who further discuss the choice of this controversial coefficient. The thermophysical properties of molten steel were taken to be constant and are summarized in Table 3. In order to avoid complications associated with unsteady free surface motion and in view of the widespread use of flux powders on top of the meniscus in the industry, the meniscus was modeled to be fixed at $z = 0$.

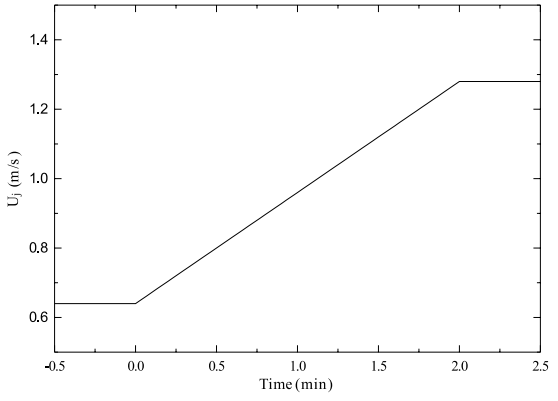

Fig. 2. Variation of the jet's exit velocity with time.

Table 3
Operating conditions of the caster and thermophysical properties of steel

Mold diameter ($2R$)	0.2032 m
Jet diameter (d_j)	0.0254 m
Mold length (L)	0.6 m
Darcy coefficient (C_0)	1.016×10^6 kg/s m^3
Ambient temperature (T_a)	30°C
Heat transfer coefficient for $z \leqslant 0.6$ m (h_1)	1163 W/m^2 K
Heat transfer coefficient for $z > 0.6$ m (h_2)	1395.6 W/m^2 K
Density of molten steel (ρ)	7.5×10^3 kg/m^3
Viscosity of molten steel (μ)	6.4×10^{-3} Ns/m^2
Specific heat (c_p)	753.624 J/kg K
Thermal conductivity (κ)	35 W/m K
Latent heat of phase change (H_f)	2.7214×10^5 J/kg
Liquidus temperature (T_ℓ)	1500°C
Solidus temperature (T_s)	1470°C
Thermal expansion coefficient (β)	10^{-3} K^{-1}

The axial velocity and the tangential derivative of the radial velocity were set to zero at the meniscus. In addition, the normal derivatives of k, ε and temperature vanish at the meniscus.

3.4. Details of the numerical scheme

A 32×60 grid system was found to be sufficient to resolve the details of the flow and temperature fields

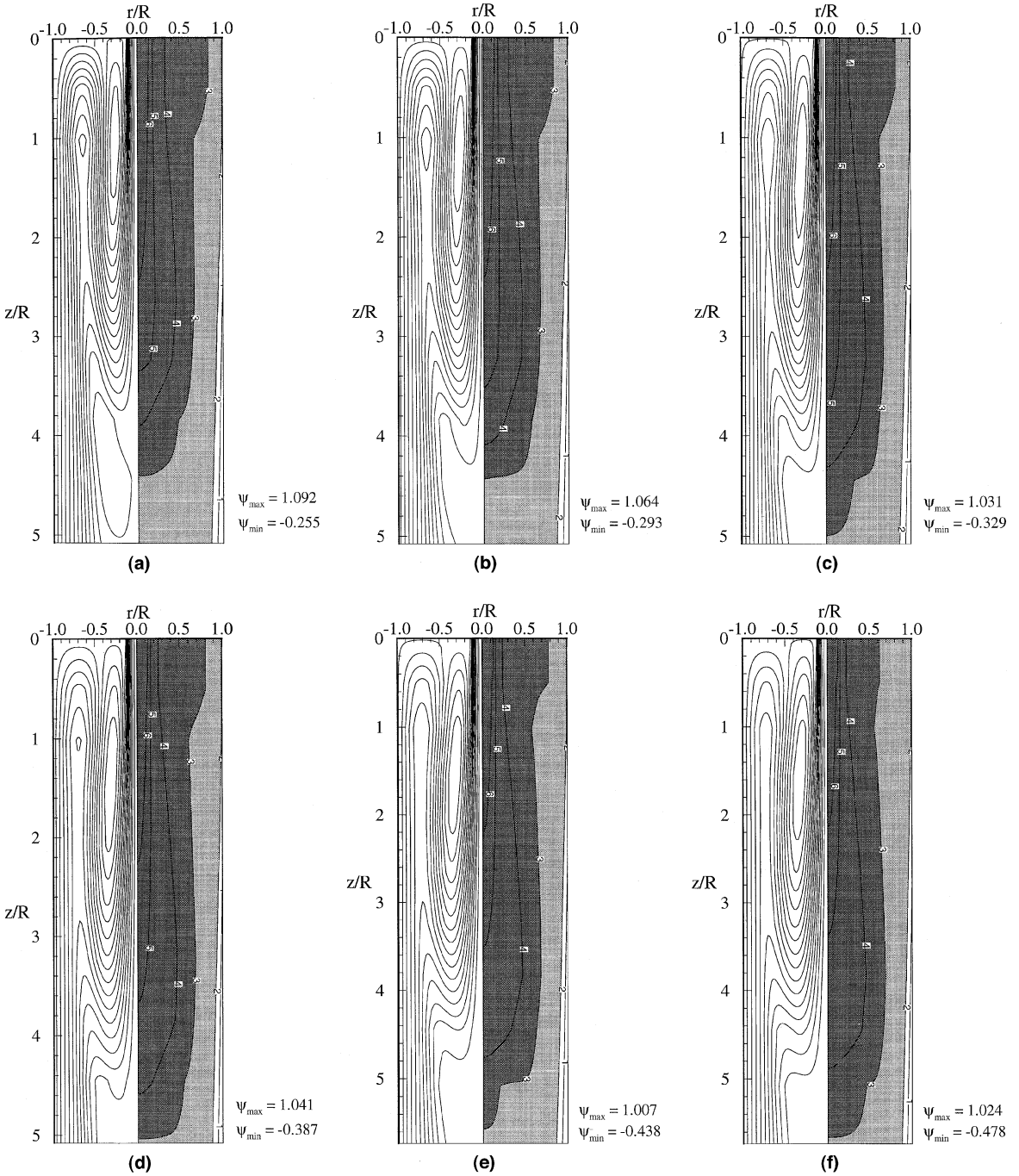

Fig. 3. Streamline patterns and temperature contours at different time instants: (a) $t = 0$, (b) $t = 10$, (c) $t = 20$, (d) $t = 30$, (e) $t = 40$, (f) $t = 50$, (g) $t = 60$, (h) $t = 70$, (i) $t = 80$, (j) $t = 90$, (k) $t = 100$, (l) $t = 110$, (m) $t = 120$, (n) $t = 130$ and (o) $t = 150$ s.

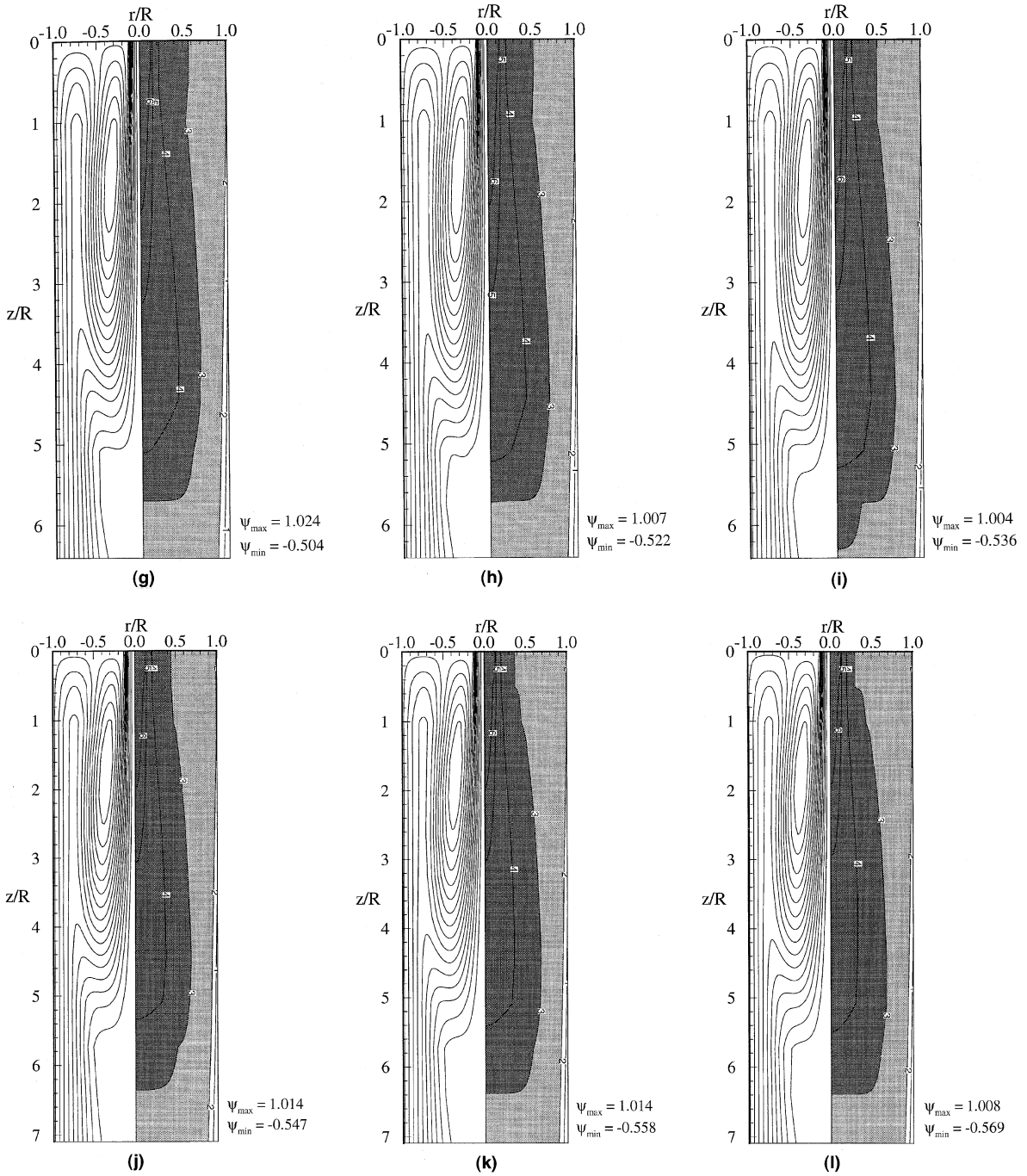

Fig. 3 (*continued*)

based on comparison of the streamline contours and liquid–solid interface positions for various grid densities under steady operating conditions. Thirty-two expanding grids (i.e., the ratio of the lengths of the successive grids is equal to a specified constant greater than 1) were employed in the streamwise direction. The radial grid layout was chosen to accommodate the presence of the shear layer and near-wall gradients. Accordingly, shrinking grids (same as expanding grids, but the constant is less than 1) were employed from the symmetry

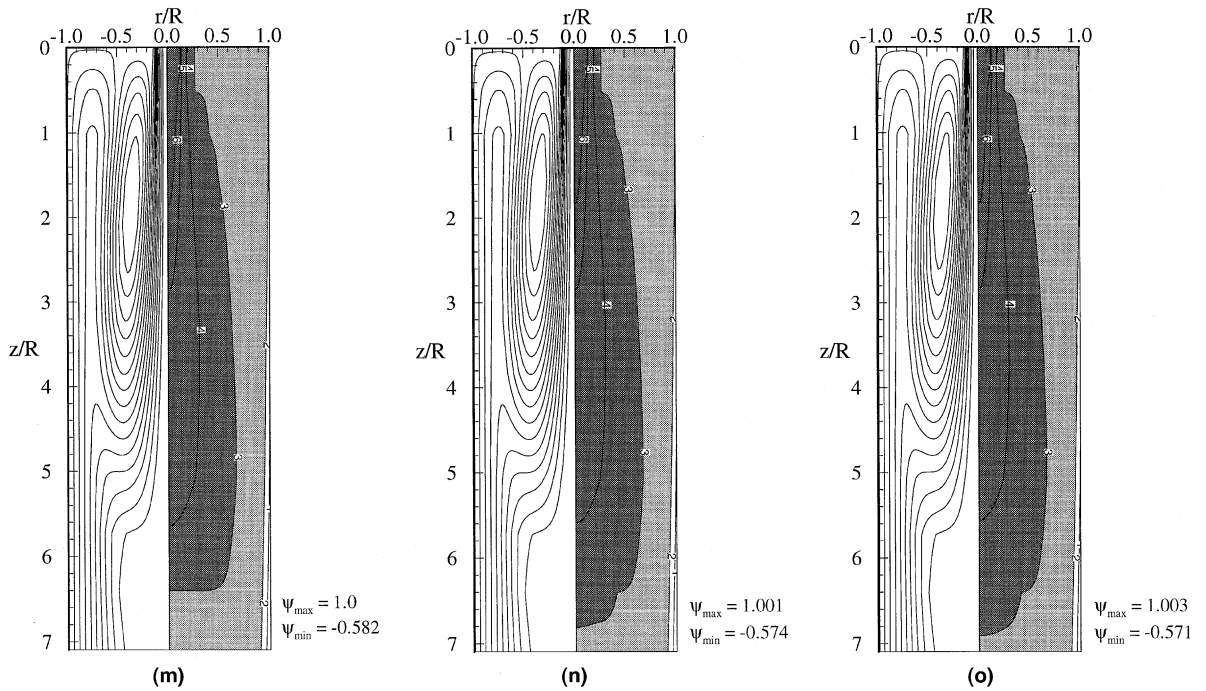

Fig. 3 (*continued*)

axis to $r = r_j$. Expanding grids were then used from $r = r_j$ to $r = 0.45R$. Finally, shrinking grids were laid from $r = 0.45R$ to the casting surface. Staggered control volumes were used for the axial and radial velocity components. All other quantities of interest were computed at the grid points. The finite-volume form of the time-averaged transport equations were obtained by adopting a semi-integral approach to discretize the equations over each control volume of the computational grid, using a hybrid-difference scheme. The line-by-line method was used to obtain converged solutions iteratively, whereas relaxation factors were employed to promote stability of the process. These parameters were 0.5, 0.45, 0.5, 0.5, 0.45, 0.3 and 0.45 for U, V, T, k, ε, μ_t and f_ℓ, respectively, whereas no relaxation was applied to the pressure correction field. The temporal derivatives were treated using an implicit formulation which demands no stability requirement and three time steps of 1, 2 and 4 s were tested. Based on the comparison among the results of the three time steps, the time step of 2 s was generally selected for the production calculations. However, difficulties in achieving convergence were encountered with this time step at certain points of the simulated time period, in which case the time step would be switched to the smaller value of 1 s. During all the transient computations, the underrelaxation parameters discussed above were maintained and the convergence criterion was set to 10^{-5}. Typically, it took about 1000–3500 iterations to converge for each time step. The CPU time per iteration was 0.107 s. The computations were carried out on the Alabama Supercomputer Network's CRAY-C90 supercomputer, which is located in Huntsville, Alabama. Greater details on numerical methodology and other aspects of the computations have been reported by Lan [19].

4. Results and discussion

The computational results pertaining to the transient flow field, heat transfer and solidification in the mold during the described grade transition practice are presented in this section. The streamline patterns, temperature contours (isotherms), time-dependence of the size of the liquid, mushy and solid regions, casting surface temperature signatures and heat flux variation along the mold are presented.

The streamline patterns and temperature contours within the mold at different instants for the tundish change simulation are shown in Figs. 3(a)–(o). The temperature contour levels in these figures (identified with aid of numbers 1–6) correspond to 1300, 1470 (equal to T_s), 1500 (equal to T_ℓ), 1510, 1520 and 1530°C, respectively. The time instants selected for presentation are 0, 10, 20, 30, 40, 50, 60, 70, 80, 90, 100, 110, 120, 130 and 150 s. At the beginning of the tundish change process (0 s), the penetration depth of the liquid pool ($T > 1500$°C) is about 4.4 mold radii. The volumes of

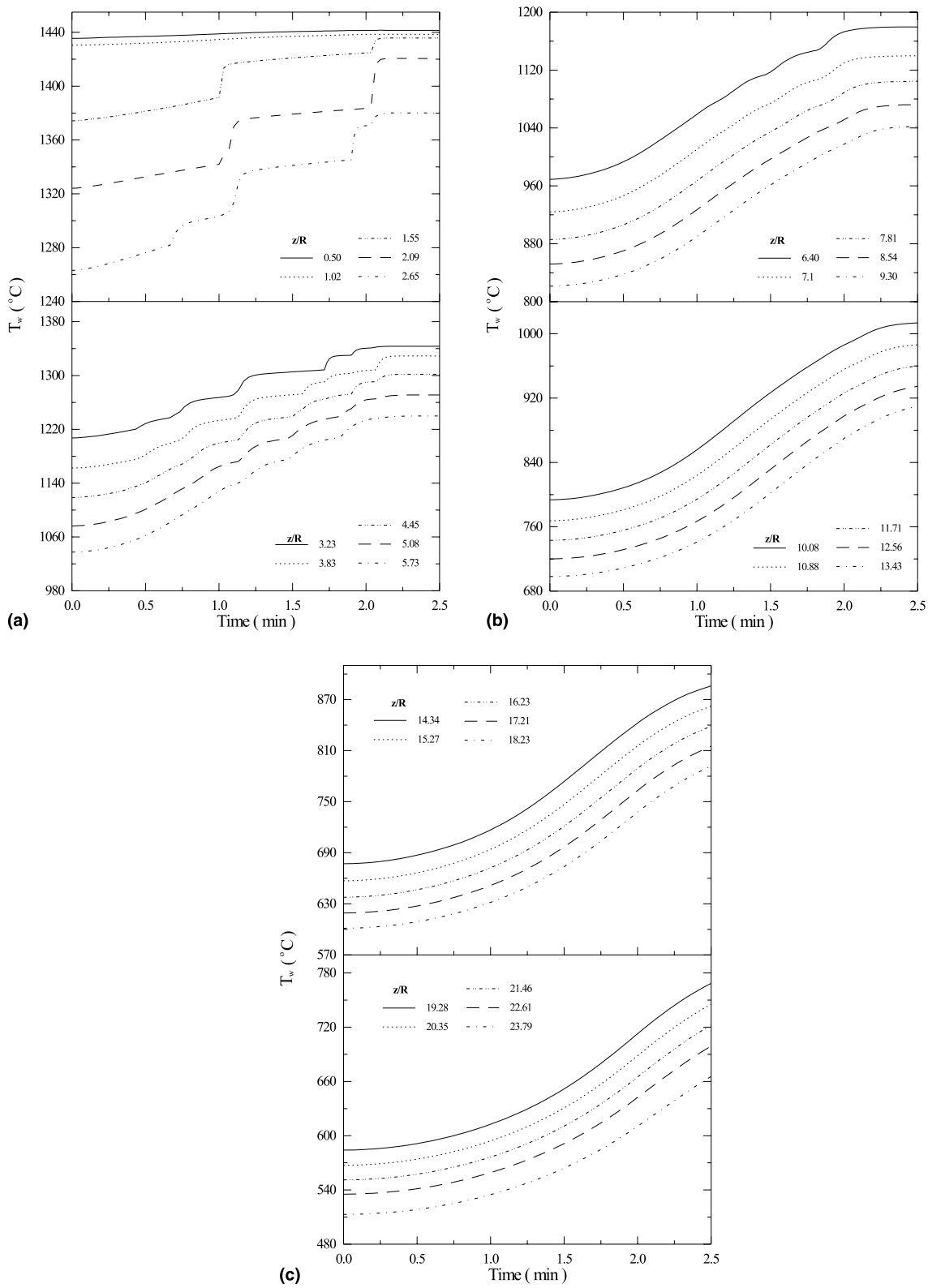

Fig. 4. Variation of the temperature of the casting surface with time at the axial grid positions: (a) 1–10, (b) 11–20 and (c) 21–30.

the liquid pool and the mushy zone within the computational domain are 6.27×10^{-3} and 3.28×10^{-2} m^3, respectively. During the first 20 s, as the jet's speed is increased, the liquid pool expands slightly near the bottom in the radial direction first and then in the axial direction significantly. After 20 s, the penetration depth of the liquid zone is 5 mold radii, up by 13.6%. Meanwhile, the upper part of the liquid pool undergoes little change. Similar behavior is observed going from 20 to 80 s. From 40 to 120 s, marked shrinkage of the liquid pool in the radial direction is observed near the inlet plane. In spite of the constant jet velocity after 120 s, the liquid zone continues to grow in the axial direction until the end of the simulated time span (150 s) because of the time lag effect. The thickness of the solid shell ($T < 1470$°C) at the bottom of the mold ($z/R = 5.91$) is of the order of 16.4% and 6.2% of the mold radius at the beginning (0 s) and end (150 s) of the simulation, respectively, decreasing significantly as the casting speed is increased.

The general features of the flow field at each time instant are similar to those of the steady-state simulations discussed previously [7] and will not be repeated. Only the time-dependent aspects of the flow field are highlighted. As the jet velocity is increased, the jet penetrates deeper in the mold due to its possession of greater momentum. As a result, the redirecting of the incoming jet takes place farther away from the inlet plane and the axial extent of the liquid zone gets longer. The increase of the jet velocity also makes the recirculatory flow stronger as evidenced by the decrease of the minimum stream function values which are identified next to each figure. The eye of the recirculation zone is continuously moving down from its initial location at $z/R = 1$ to about 1.8 at the end of the ramping of the casting speed. At low jet velocity when the buoyancy effect is more dominant, more incoming liquid jet rises and moves sideways in the area near the inlet plane, causing greater convection heat transfer in this area and thus growth of liquid zone in the radial direction. As the jet velocity increases, convection effect becomes less pronounced in this region and consequently the liquid pool shrinks in the radial direction.

The influence of the time-dependence of the inlet jet velocity on the temperature of the surface of the casting is shown in Fig. 4(a)–(c). Instantaneous casting surface temperature values are given at various axial stations within the mold ($z/R < 5.91$) and below the mold where the water sprays are located ($z/R > 5.91$). The variation of the temperature of the surface of the casting with time followed the trends of the jet velocity (Fig. 2). Despite the uniform increase of the jet velocity over the ramping period, around 60–70 and 110–130 s and at certain axial locations ($1.55 \leqslant z/R \leqslant 2.65$), sharp temperature rise signatures are observed. These distinct temperature rise signatures are associated with axial stations where the radial thickness of the mushy zone is small (Figs. 3(g), (h), (l), (m) and (n)) and the radial growth of the liquid pool with time promotes greater conduction heat transfer through the thinning mushy zone. Inspection of Figs. 4(a)–(c) also reveals that at the end of the ramping of the casting speed (120 s) the casting surface temperatures at the stations in the upper part of the computational domain ($0.5 \leqslant z/R \leqslant 7.1$) basically do not change as the time passes by, whereas the casting surface temperatures at the bottom stations of the solution domain ($14.34 \leqslant z/R \leqslant 23.79$) continue to rise, which explains the continuing expansion of the liquid zone at the end of the ramping of the casting speed pointed out earlier.

Instantaneous local surface heat flux values ($q_w(z,t) = -\kappa \frac{\partial T}{\partial r}|_{r=R}$) at every axial station were evaluated. Since the heat transfer coefficients are constant, the changes of the local surface heat flux values with time are directly proportional to the changes of the surface temperature with time discussed above. Thus, the trend of the local surface heat flux variation with time is identical to that of the surface temperature (Figs. 4(a)–(c)). The local increase of the local heat flux values at the bottom of the mold ($z/R = 5.91$) due to the switch to the spray cooling was also clearly observed.

The variation of the bulk heat flux ($q_b = \int_0^L q_w(z,t)\, dz/L$) which is made dimensionless with $q_0 = \kappa(T_\ell - T_s)/R$ with time is shown in Fig. 5. The heat removal rate by the mold increases almost linearly with the ramping of the casting speed. At the end of the tundish change operation (120 s), the bulk mold heat flux still increases for about another 10 s and then reaches a constant value.

The variations of the dimensionless volumes of the liquid and mushy zones with time are presented in Fig. 6. The instantaneous volumes of the liquid and mushy zones are non-dimensionalized with their values at $t = 0$ s. The volume of the liquid pool increases almost linearly to about 115% of its initial size over a time duration of 30 s. It then remains fairly constant for the remainder of the tundish change operation while

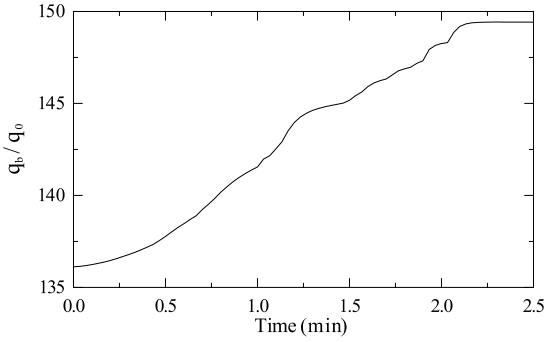

Fig. 5. Variation of the bulk mold heat flux with time.

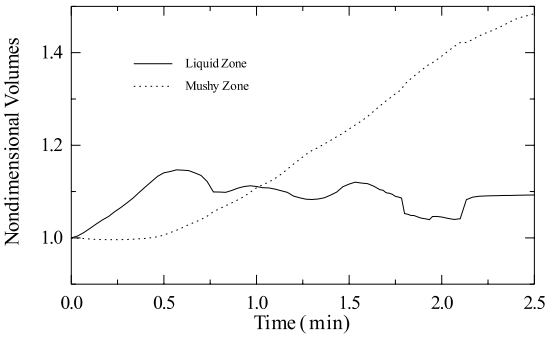

Fig. 6. Variation of the dimensionless volumes of the liquid and mushy zones with time.

experiencing some shrinkage around 110 s. In contrast, the volume of the mushy zone almost stays constant during the first 30 s, and then increases approximately linearly all the way to about 148% of its initial size at the end of the simulated time span.

In order to quantify the variation of the solidified shell with time, the deviation of the thickness of the solid shell from its value at $t = 0$ was defined as

$$\text{Deviation} = \left[\frac{1}{N} \sum_{i=1}^{N} \left(\frac{r_0(i) - r(i)}{R} \right)^2 \right]^{0.5}, \qquad (10)$$

with $r_0(i)$ and $r(i)$ representing the $t = 0$ and instantaneous radial coordinates of the points on the solidus line at the ith axial computational station, respectively. The quantity N is the total number of calculation stations in the axial direction. The deviation of the thickness of the solid is shown in Fig. 7. Since the deviation is defined just to measure the overall relative variation of the solid shell thickness from its initial value and as always being positive (Eq. (10)), the decrease of the solidified shell thickness for the tundish change operation is seen as increase of the deviation in Fig. 7. The variation of the shell thickness with time followed the trend of the jet velocity. As the jet velocity increases, the shell thickness decreases monotonically and at the end of the simulated time period the deviation of the solid shell thickness from its initial value is about 32.8. This suggests that during the tundish change operation thinning of the solid shell is very significant and must be taken into consideration to prevent breakout from occurring.

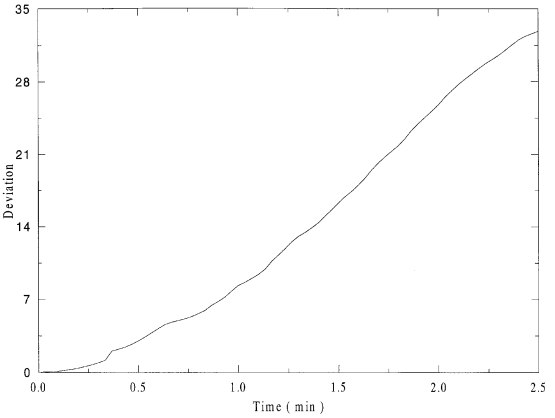

Fig. 7. Deviation of the thickness of the solid shell from its initial value at various time instants.

5. Conclusions

Based on the findings of the computational study presented in this paper, the following conclusions are drawn:

1. In spite of the transient nature of the incoming liquid steel velocity, increase in size of the liquid pool with time during the tundish change operation is observed to be insignificant, whereas the increase of the volume of the mushy zone is very marked and is as much as 48% relative to its initial size.
2. Distinct casting surface temperature rise signatures were detected for the tundish change operation. The heat removal rate from the mold increases almost linearly similar to the ramping of the casting speed.
3. Thinning of the solidified shell during tundish change is significant in comparison to the ladle change operation and must be taken into account in practice to prevent breakout.

Acknowledgements

This research was supported by the CRAY Research, Inc., Eagan, MN through two University Research & Development Grant Program grants. The first author also acknowledges the financial support of the Advanced Manufacturing Technology Center and the Engineering Experiment Station at Auburn University. The opportunity of using the computer facilities/services of the Alabama Supercomputer Network is greatly appreciated.

References

[1] J. Szekely, R.T. Yadoya, The physical and mathematical modeling of the flow field in the mold region in continuous casting systems: Part I. Model studies with aqueous systems, Metall. Trans. 3 (1972) 2673–2680.

[2] J. Szekely, R.T. Yadoya, The physical and mathematical modeling of the flow field in the mold region in continuous

casting systems: the mathematical representation of turbulent flow (Part II), Metall. Trans. 4 (1973) 1379–1388.
[3] J.M. Khodadadi, Y. Liang, F. Shen, Physical modeling of the turbulent flow in the mold of continuous casters using an aqueous system, AFS Trans. (1991) 421–428.
[4] W. Shyy, Y. Pang, G.B. Hunter, D.Y. Wei, M.-H. Chen, Modeling of turbulent transport and solidification during continuous ingot casting, Int. J. Heat Mass Transfer 35 (5) (1992) 1229–1245.
[5] W. Shyy, Y. Pang, G.B. Hunter, D.Y. Wei, M.-H. Chen, Effect of turbulent heat transfer on continuous ingot solidification, Trans. ASME J. Engrg. Mater. Technol. 115 (1993) 8–16.
[6] M. Reza Aboutalebi, M. Hasan, R.I.L. Guthrie, Coupled turbulent flow, heat and solute transport in continuous casting processes, Metall. Mater. Trans. B 26 (4) (1995) 731–744.
[7] X.K. Lan, J.M. Khodadadi, Fluid flow, heat transfer and solidification in the mold of continuous casters during ladle change, Int. J. Heat Mass Transfer 44 (5) (2001) 953–965.
[8] X. Huang, B.G. Thomas, Modeling of steel grade transition in continuous slab casting processes, Metall. Trans. B 24 (1993) 379–393.
[9] B.G. Thomas, Modeling study of intermixing in tundish and strand during a continuous-casting grade transition, in: Steelmaking Conference Proceedings, Iron & Steel Society of AIME, 1996, pp. 519–531.
[10] Y.-H. Ho, W.-S. Hwang, Analysis of molten steel flow in billet continuous casting mold, ISIJ Int. 36 (8) (1996) 1030–1035.
[11] X. Huang, B.G. Thomas, Modeling of transient flow phenomena in continuous casting of steel, Can. Metall. Quart. 37 (3&4) (1998) 197–212.
[12] S.V. Patankar, in: Numerical Heat Transfer and Fluid Flow, Hemisphere, Washington, DC, 1980.
[13] C.K.G. Lam, K. Bremhorst, A modified form of the k–ε model for predicting wall turbulence, Trans. ASME J. Fluids Engrg. 103 (1981) 456–460.
[14] V.C. Patel, W. Rodi, G. Scheuerer, Turbulence models for near-wall and low Reynolds number flows: a review, AIAA J. 23 (1985) 1308–1319.
[15] X.K. Lan, J.M. Khodadadi, F. Shen, Evaluation of six k–ε turbulence model predictions of flow in a continuous casting billet-mold water model using laser doppler velocimetry measurements, Metall. Mater. Trans. B 28 (2) (1997) 321–332.
[16] V.R. Voller, C. Prakash, A fixed grid numerical modelling methodology for convection–diffusion mushy region phase-change problems, Int. J. Heat Mass Transfer 30 (8) (1987) 1709–1719.
[17] V.R. Voller, A.D. Brent, C. Prakash, Modelling the mushy region in a binary alloy, Appl. Math. Modelling 14 (1990) 320–326.
[18] The Iron and Steel Institute of Japan, Handbook of Physico-Chemical Properties at High Temperatures, Special Issue No. 41, ISIJ, Japan.
[19] X.K. Lan, Computational and experimental investigation of transport phenomena in a continuous casting mold, Ph.D. Thesis, Auburn University, Auburn, AL, 1998.